Evaluation of Extraction and Enhancement of Response due to Target Inhomogeneities for Resistivity Interpretation

by

Tsuyoshi SUGANO* and Koichi SASSA*

(Received September 26, 1988)

Abstract

The future effectiveness of the resistivity method depends upon its ability to interpret field data obtained under more complex geological structure environments. Generally, the effects of nontarget surroundings such as weathered overburden layers, vertical contacts, faults, fracture zones, deep bed rocks or host rocks, near-surface lateral or local inhomogeneities and topography are noises for exploration, and only the response due to the target is a signal. In these various resistivity environments, it is very important to know how to reduce the nontarget inhomomeneity effects. Also, one must be careful when applying the homogeneous medium interpretation techniques to actual field data processing.

In this paper, the following points are discussed;

(1) Normalization of the noises caused by geologic structures in order to extract and enhance the response (signal) due to the target inhomogeneities.

(2) Significance of expression procedure in an evaluation of resistivity interpretation process and results.

(3) Sensitivity distribution newly developed by using the FEM 2D-3D algorithm in the case of nontarget inhomogeneities. Also, the sensitivity difference of its application that is effective to evaluate the extraction and enhancement of the response (signal) due to the target inhomogeneities in various surroundings.

1. Introduction

New electrical prospecting methods utilizing the three-dimensional data and subsurface electrodes have become increasingly important exploration tools for

*Department of Mineral Science and Technology

detecting deeply located mineral or low mineralized deposits, energy and groundwater reservoirs and geological fracture zones.[1)14-18)20)27)30)]

The most important recent developments in the electrical technique include the uses of high density numerical modelings and three-dimensional subsurface electrodes.[4-5)8)14-15)20)30)]

In general, although field measurements are carried out under complicated subsurface structures, the interpretation of resistivity prospecting data may be commonly performed by employing the techniques developed by assuming homogeneous ground. Recently, the development of the computer 2D-3D or 3D modeling has provided us with a very powerful tool for a more quantitative investigation in the cases of various inhomogeneities.

In the present study, first, the response due to target inhomogeneities in various surroundings has been investigated by using the finite element method (FEM) 2D-3D algorithm. Next, four examples of its application have been chosen to give an aid to a more effective resistivity interpretation, and to be most interesting from the view points of interactive modeling and visualization systems:

(1) Normalization procedure of the noises caused by geologic structures in order to extract and enhance the response (signal) due to the target inhomogeneities.

(2) Solid electrode array method using cross-hole (or hole-to-hole) and hole-to-surface (and/or surface-to-hole) configurations.

(3) Expression procedure in an evaluation of resistivity interpretation process and results.

(4) Sensitivity distribution newly developed using the FEM 2D-3D algorithm in the case of nontarget inhomogeneities, and the sensitivity difference applied to evaluate the degree of extraction and enhancement of the response (signal) due to the target inhomogeneities in various resistivity soundings.

Section 2 gives apparent resistivity of an arbitrary three-dimensional electrode array calculated by the FEM 2D-3D algorithm. Sections 3 and 4 give normalization results to reduce the nontarget inhomogeneity effects for extraction and enhancement of the response (signal) due to the target inhomogeneities, and the significance of the expression procedure in an evaluation of the resistivity interpretation process. Section 5 gives a sensitivity distribution in nontarget inhomogeneities and its application. Finally, section 6 gives conclusions.

2. Apparent resistivity calculated using FEM 2D-3D algorithm for three-dimensional electrode array

Recently, the finite element 2D-3D modeling algorithm for electrical and electromagnetic methods introduced by Coggon (1971), Rijo (1977) etc.[2-3], and developed by many resistivity studies, has become a flexible tool for quantitative interpretation.

Generally, to reduce the errors in finite element modeling, it is a common practice to make the mesh finer near the sources and the inhomogeneities. However, one would need more computer time with the finer mesh. We have also suggested, as Zhao, Rijo and Ward (1986)[4] did, that the normalization procedure is very useful to compensate the errors due to the discrete nature of the finite element mesh and also due to the inverse Fourier transform.

In order to discuss the effectiveness of the normalization procedure to compensate the error in the finite element solution, two kinds of sensitivity have been defined[6] as:

$$\left.\begin{aligned} S_{k,FEM} &= (\rho_{ak,FEM}-\rho_{a0,FEM})/\rho_{a0,FEM} \cdot 100, \\ S_{k,ANALYT} &= (\rho_{ak,ANALYT}-\rho_{a0,ANALYT})/\rho_{a0,ANALYT} \cdot 100, \end{aligned}\right\} \qquad (1)$$

where,

$S_{k,FEM}$=sensitivity (%) obtained from the FEM solution,
$S_{k,ANALYT}$=sensitivity (%) obtained from the analytical solution,
$\rho_{ak,FEM}$=apparent resistivity(ohm-m) of the inhomogeneous earth with target inhomogeneities computed by the FEM,
$\rho_{a0,FEM}$=apparent resistivity(ohm-m) of the homogeneous half-space computed by the FEM,
$\rho_{ak,ANALYT}$=apparent resistivity(ohm-m) of the inhomogeneous earth with target inhomogeneities by the analytical method,
$\rho_{a0,ANALYT}$=apparent resistivity(ohm-m) of the homogeneous half-space by the analytical method.

By definition, the sensitivities in the cases of $S_k \lesseqgtr 0$ for the relation of $\rho_k \lesseqgtr \rho_0$ between the target resistivity ρ_k and the homogeneous half-space resistivity ρ_0 are called the normal sensitivity. Those in the case of $S_k \gtreqless 0$ for the same resistivity relation are called the reverse sensitivity, respectively.

From expression (1), we have newly defined a sensitivity difference ΔS_k

and a normalization factor n. Those are as follows:

$$\Delta S_{k,\,FEM/ANALYT}=S_{k,\,FEM}-S_{k,\,ANALYT}, \tag{2}$$

$$n=V_{a0,\,FEM}/V_{a0,\,ANALYT}=\rho_{a0,\,FEM}/\rho_{a0,\,ANALYT}. \tag{3}$$

By applying these equations, the apparent resistivity $\rho_{ak,\,ANALYT}$ is given by the following expression, namely,

$$\rho_{ak,\,ANALYT}=\rho_{ak,\,FEM}/n-\Delta S_{k,\,FEM/ANALYT}\cdot\rho_{a0,\,ANALYT}. \tag{4}$$

It may be considered that the sensitivity difference ΔS_k changes with both the characteristics of the geological models and the electrode configuration. In a case where the sensitivity difference ΔS_k is negligible, we can obtain the normalized apparent resistivity ($\rho^n_{ak,\,FEM}$) from the $\rho_{ak,\,FEM}$ by using the following relation,

$$\rho^n_{ak,\,FEM}=\rho_{ak,\,FEM}/n. \tag{5}$$

From these results, the normalized apparent resistivity obtained by expression (5) becomes the approximate apparent resistivity with the error $\Delta S_{k,\,FEM/ANALYT}\cdot\rho_{a0,\,ANALYT}$, which is the second term on the right side in Equation (4). Zhao, Rijo and Ward (1986)[4] reported that the error in the unnormalized FEM solution was in the range from 6% to approximately 42% in the case of the infinite, very thin, conductive dike model in a half-space. They also clarified that the error in the solution normalized by the finite element solution of the half-space was in the range from 0.1% to 3% and the mean-square error was reduced from 25% to 1.9% by the normalization.

Figure 1 illustrates an example of the normalization factor distribution obtained by the FEM 2D-3D algorithm for the homogeneous model of which resistivity is 100 ohm-m. The values are computed for the so-called quasi three-dimensional, namely the 2D-3D model of which the dimensions are a width of 6800 m in the x-direction, a length of 3000 m in the y-direction (the strike direction) and a depth of 3200 m in the z-direction. They are shown as maps and sections. The electrode configuration illustrated in Figure 1 is C (I) (700, 1100, -200) P (V) (x, y, 0) hole-to-surface solid array. This normalization factor distribution may change according to a change of the simulation model.

Figure 2 illustrates the sensitivity difference pseudo-map for C (700, 1100, -200) P (surface) solid electrode array calculated by Equation (2) in the case of the vertical three-layers model. The model has a vertical conductive vein at the middle, namely, in Figure 3, $\rho_1=\rho_2=\rho_4=$ 100 ohm-m and the resistivity ρ_3 of the outcropped vertical vein with a thickness 200 m (from 900 m to 1100 m in the x

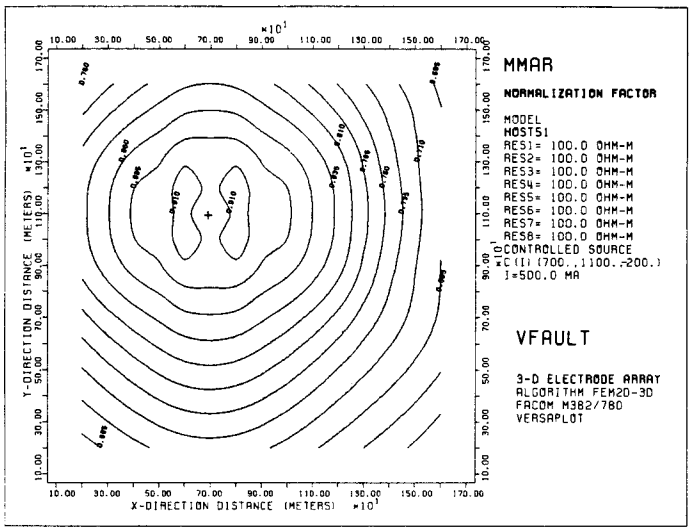

Fig. 1. An example of the normalization factor distribution.

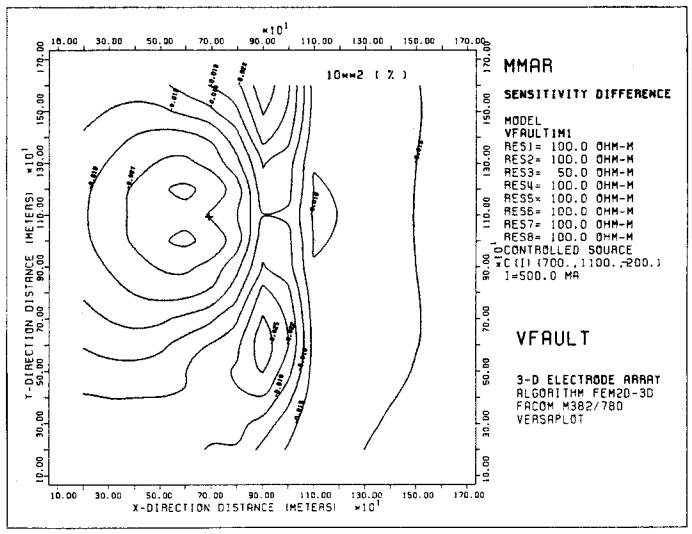

Fig. 2. A sensitivity difference distribution of C(subsurface) P(surface) cross-hole electrode array configuration in the case of the vertical three-layers model.

-direction) is 50 ohm-m. The sensitivity difference ΔS_k is in the range from -2.5% to -0.4%.

It shows that the errors can be reduced considerably by the normalization

procedure. Also, the apparent resistivity which is approximately equal to the analytical solution can be obtained sufficiently. However, by comparing Figure 1 with Figure 2, we see that all positions showing large sensitivity differences do not agree with those showing large differences of the normalization factor n to 1.0. This result indicates that the sensitivity difference may change according to the characteristics of structure and the location of the current source.

3. Normalization procedure to reduce the nontarget inhomogeneity effects for extraction and enhancement of the response (signal) due to target inhomogeneities

Generally, in the complex resistivity environments, it is very important how to reduce the various nontarget inhomogeneity effects for the extraction and enhancement of the response (signal) due to the target inhomogeneities.[6]

We have already defined the sensitivity difference in expression (2) in order to evaluate the performance of the FEM 2D-3D numerical modeling system. Here, we have applied the concept of sensitivity difference to an evaluation of the normalization procedure to extract and enhance the response (signal) of the target inhomogeneities. The new sensitivity in the nontarget inhomogeneities is defined as:

$$S_{kN/N}=(\rho_{akN}-\rho_{aN})/\rho_{aN}\cdot 100, \tag{6}$$

where,

$S_{kN/N}$=sensitivity (%) for the nontarget inhomogeneities,
ρ_{akN}=apparent resistivity (ohm-m) of the inhomogeneous earth structure which consists of target and nontarget inhomogeneities and
ρ_{aN}=apparent resistivity (ohm-m) of the nontarget inhomogeneities.

Next, in the case of target inhomogeneities existing in the half-space homogeneous medium, the sensitivity was given[1)9-11)] by,

$$S_k=(\rho_{ak}-\rho_{a0})/\rho_{a0}\cdot 100, \tag{7}$$

where,

S_k=sensitivity (%) for the half-space homogeneous medium,
ρ_{ak}=apparent resistivity (ohm-m) of the homogeneous medium with target inhomogeneities and
ρ_{a0}=apparent resistivity (ohm-m) of the homogeneous medium.

Now, a new sensitivity difference $\Delta S_{kN/N}$ between the sensitivity $S_{kN/N}$ for the nontarget inhomogeneities and the sensitivity S_k for the homogeneous medium is defined as:

$$\Delta S_{kN/N}=S_{kN/N}-S_k. \tag{8}$$

Therefore, from expressions (6), (7), and (8), the new apparent resistivity ρ_{ak} can be expressed as:

$$\rho_{ak}=(\rho_{akN}/\rho_{aN})\cdot\rho_{a0}-\Delta S_{kN/N}\cdot\rho_{a0}. \tag{9}$$

If the second term $\Delta S_{kN/N}\cdot\rho_{a0}$ on the right side in Equation (9) is negligible compared with the first term, we can obtain the apparent resistivity ρ^n_{ak} which is normalized by the apparent resistivity of the nontarget inhomogeneities as follows:

$$\rho^n_{ak}=(\rho_{akN}/\rho_{aN})\cdot\rho_{a0}. \tag{10}$$

As shown above, the sensitivity difference $\Delta S_{kN/N}$ in Equation (9) can be applied to evaluate the degree of the extraction and enhancement of the target response in the normalization procedure to reduce the nontarget inhomogeneity effects. It may also be used in order to estimate and evaluate the interpretation process and results in the interactive quantitative analysis.

Figure 3 shows an inhomogeneous earth model with a single conductive vertical target and its surroundings, which consist of a vertical contact and a partial horizontal overburden.

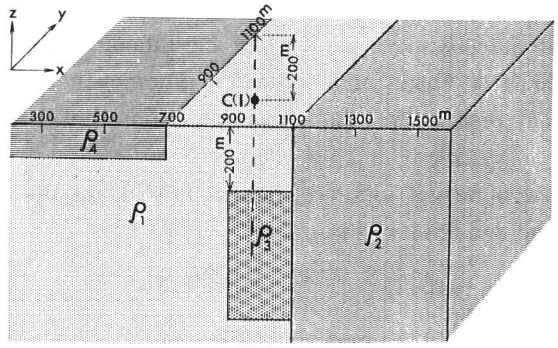

Fig. 3. An example of resistivity model which consists of a conductive vertical target and its surroundings including a vertical contact and a partial horizontal overburden.

A geological model having a conductive vertical target is made by setting ρ_1 = 700 ohm-m, ρ_2= 100 ohm-m, ρ_3= 10 ohm-m and ρ_4= 200 ohm-m for the model in Figure 3. This model is called Model 5171 W. In order to get the apparent resistivity distribution within this model, a current electrode C (I) is located at x= 700 m, y= 1100 m, z= − 200 m. Figure 4 shows the apparent resistivity distributions computed by using the FEM 2 D- 3 D algorithm for Model 5171 W and for C (700, 1100, − 200) P (subsurface) cross-hole (or hole-to-hole) solid electrode array. Figure 4 a shows the xz section in which current electrode is located. Figures 4 b and 4 c show the xz sections of 200 m and 400 m apart from the current source in the y-direction (the strike direction), respectively.

As the xz section distance from the source becomes longer, the maximum value near the source disappears and the minimum value of about 83 ohm-m at the source side near the target becomes higher, up to about 108 ohm-m. Also, 383 ohm-m near the horizontal overburden becomes smaller to about 333 ohm-m. (Compare Figs. 4 a, 4 b, and 4 c.) The response due to the conductive vertical target has been greatly disturbed by the geologic effects of a vertical contact and a horizontal overburden.

The apparent resistivity sections shown in Figures 4 a, 4 b, and 4 c are normalized by the apparent resistivities in the nontarget inhomogeneities model which is made by setting ρ_1=ρ_3= 700 ohm-m, ρ_2= 100 ohm-m and ρ_4= 200 ohm-m. This nontarget inhomogeneities model is called Model 71 W. Figures 5 a, 5 b, and 5 c show the normalized apparent resistivity sections. For references, the apparent resistivity sections in the model having only a single conductive vertical target named as Model 51, that is, ρ_1=ρ_2=ρ_4= 100 ohm-m and ρ_3= 10 ohm-m, are shown in Figures 6 a, 6 b, and 6 c.

Comparing Figure 5 a with Figure 6 a, it was found that the minimum value of about 55 ohm-m which is produced in the upper left corner of the target in the case of Model 51 (see Fig. 6 a) was greatly enhanced in the normal sensitivity up to the minimum value of about 20 ohm-m in the normalized apparent resistivity section. (See Fig. 5 a.) The same tendencies may be also seen in the apparent resistivity values of other xz sections shown in Figures 5 b and 6 b, and also in Figures 5 c and 6 c.

From these results, it has been clear that the normalization procedure was very useful to reduce the effects of nontarget inhomogeneities surrounding the target body and to extract and enhance the response due to the target.

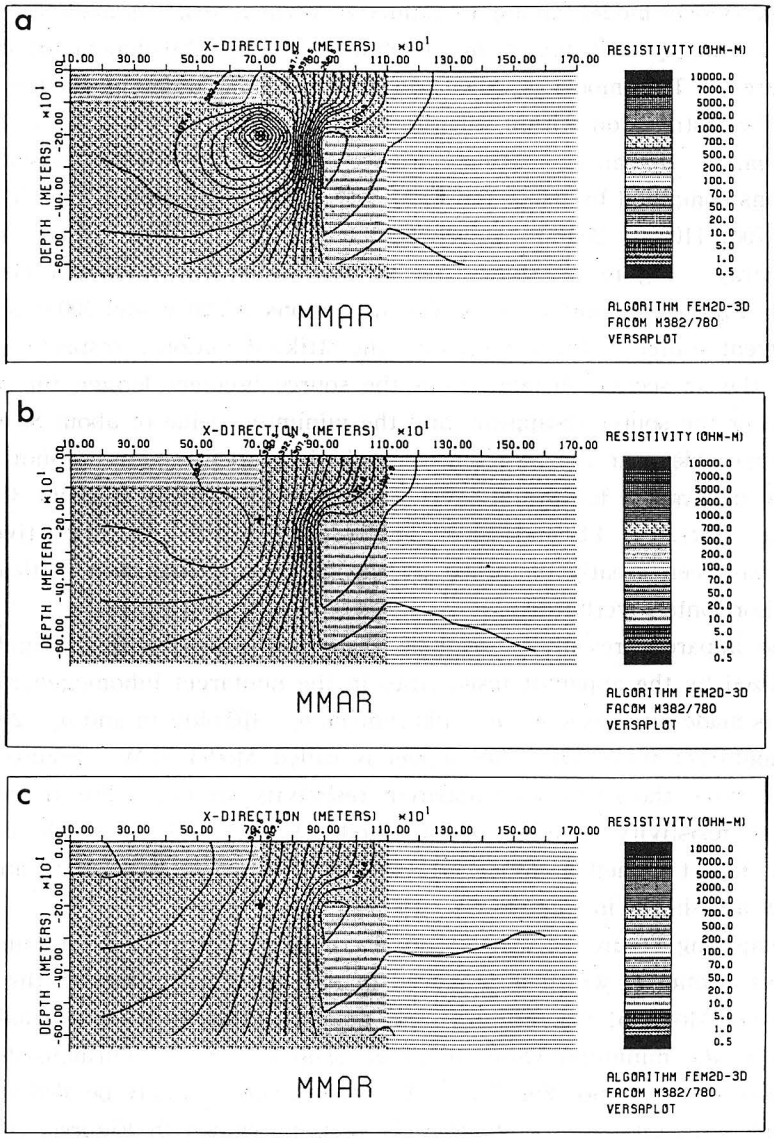

Fig. 4. C(subsurface) P(subsurface) cross-hole apparent resistivity contour sections in the case of Model 5171W (ρ_1=700 ohm-m, ρ_2=100 ohm-m, ρ_3=10 ohm-m and ρ_4=200 ohm-m in Fig. 3).
(a) : *xz* section with the source C(I), (b) : *xz* section at the distance 200m from C(I), (c) : *xz* section at the distance of 400m from C(I).

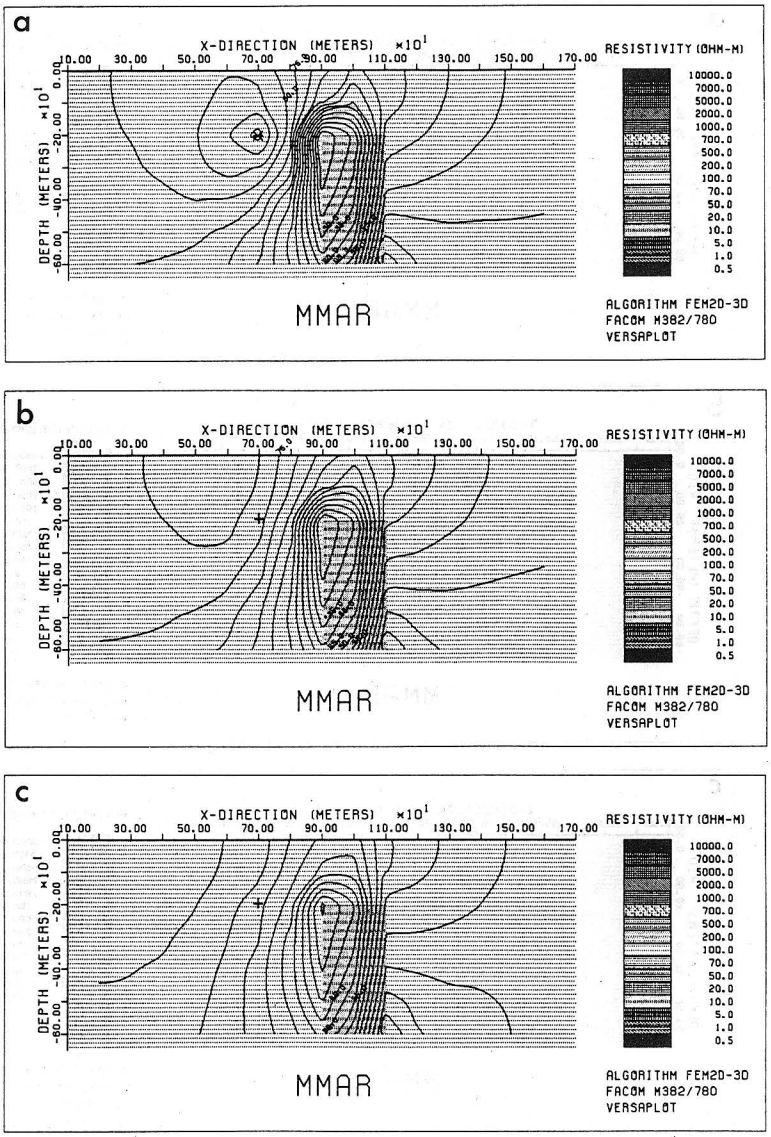

Fig. 5. Apparent resistivity contour sections normalized by the nontarget inhomogeneities model (Model 71W, $\rho_1=\rho_3=700$ ohm-m, $\rho_2=100$ ohm-m and $\rho_4=200$ ohm-m in Fig. 3). (a) : xz section with the source C(I), (b) : xz section at the distance 200m from C(I), (c) : xz section at the distance 400m from C (I).

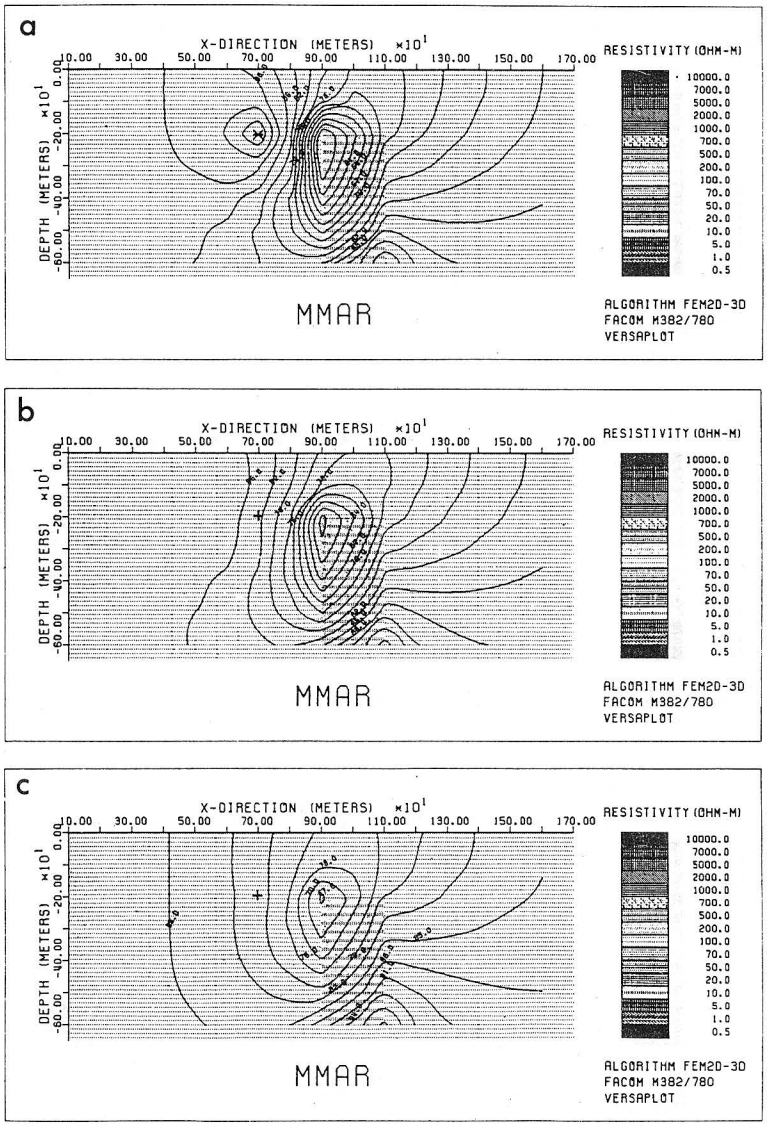

Fig. 6. C(subsurface) P(subsurface) cross-hole apparent resistivity contour sections in the case of Model 51($\rho_1=\rho_2=\rho_4=100$ ohm-m and $\rho_3=10$ ohm-m in Fig. 3). (a) : xz section with the source C(I), (b) : xz section at the distance of 200m from C(I), (c) : xz section at the distance of 400m from C(I).

4. Significance of expression procedure in an evaluation of resistivity interpretation process

In this section, the significance of the expression procedure in an evaluation of the resistivity interpretation process and results is discussed using examples of the normalization procedure applied to cross-hole (or hole-to-hole) and hole-to-surface (and/or surface-to-hole) solid electrode array resistivity modelings for a more complicated structure than that of section 2. The new model studied

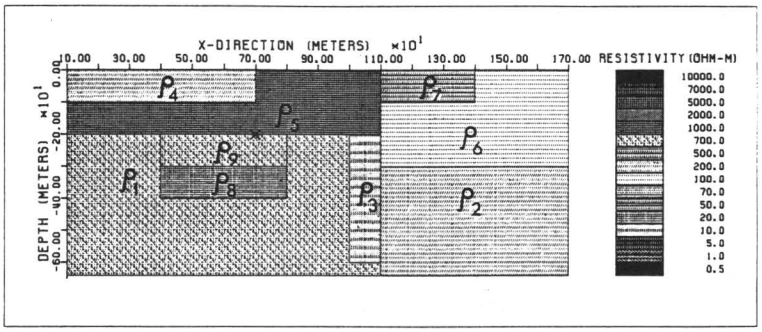

Fig. 7. An example of complicated resistivity model which consists of a conductive vertical target and its surroundings including a vertical contact, partial horizontal overburden, a deep horizontal layer, near-surface local inhomogeneity and local structure near the source C(I).

here, as shown in Figure 7, has the following conditions:

(1) A thin, conductive vertical target inhomogeneity of which resistivity ρ_3 = 10 ohm-m.

(2) A deep horizontal layer at the right-side of a vertical contact.

(3) A near-surface local inhomogeneity.

(4) Nontarget inhomogeneities with large resistivity contrast above the current source.

Figure 8 a illustrates the apparent resistivity contour in xz section with the current source in the case of C (700, 1100, − 200) P (subsurface) cross-hole array for the complex inhomogeneities model shown in Figure 7, namely, ρ_1= 700 ohm-m, ρ_2= 200 ohm-m, ρ_3= 10 ohm-m, ρ_4= 200 ohm-m, ρ_5= 1000 ohm-m, ρ_6= 100 ohm-m, ρ_7= 500 ohm-m, ρ_8= 20 ohm-m and ρ_9= 700 ohm-m. This model is called Model 5272 WLN. Figure 8 b shows the apparent resistivity contour in the same section for the model similar to Model 5272 WLN. This model is called Model 5272 WLC. The resistivities are the same except ρ_9= 20 ohm-m in Figure 7.

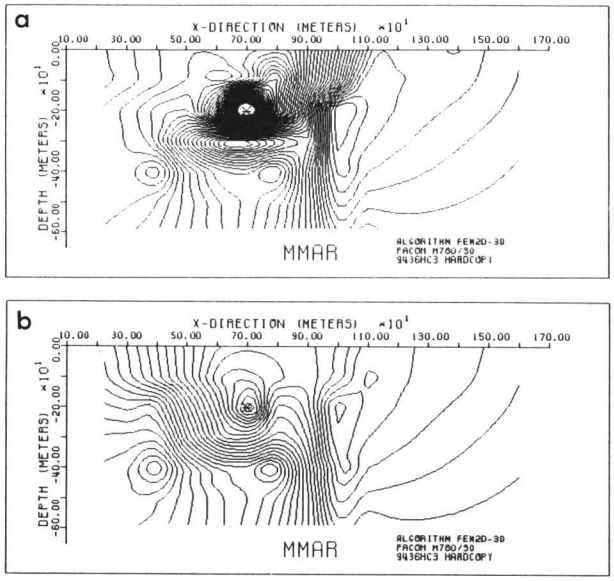

Fig. 8. C(subsurface) P(subsurface) cross-hole apparent resistivity contour sections. (a) : Model 5272WLN ($\rho_1=\rho_9=700$ ohm-m, $\rho_2=\rho_4=200$ ohm-m, $\rho_3=10$ ohm-m, $\rho_5=1000$ ohm-m, $\rho_6=100$ ohm-m, $\rho_7=500$ ohm-m, $\rho_8=20$ ohm-m and $\rho_9=700$ ohm-m in Fig. 7), (b) : Model 5272WLC (same as Model 5272WLN except $\rho_9=20$ ohm-m in Fig. 7).

Comparing Figure 8 a with 8 b, we see that the effect of the noise caused by near-source inhomogeneities is interestingly very large. However, Figure 8 a is similar to 8 b at the right-side of the target and also beneath the near-source noise structure. It suggests to us that one can select the electrode configurations so as to decrease the effects of nontarget inhomogeneities.

Figures 9 a and 9 b illustrate three-dimensional perspective views of apparent resistivity distributions. These perspective views of the plot are very helpful in the resistivity interpretation process of large three-dimensional data as well as the two-dimensional contour plot as an aid to the experts.

In the iterative interpretation process, one can monitor and evaluate every stage of analysis using recent computer simulation techniques.

At first, let us normalize the results shown in Figure 8 a and 8 b by the apparent resistivity distributions of the nontarget inhomogeneities models called Model WLN and Model WLC, respectively. Model WLN was made by setting the respective resistivity shown in Figure 7 as follows, $\rho_1=\rho_2=\rho_3=\rho_6=100$ ohm-m, $\rho_4=200$ ohm-m, $\rho_5=1000$ ohm-m, $\rho_7=500$ ohm-m, $\rho_8=20$ ohm-m and $\rho_9=700$ ohm-

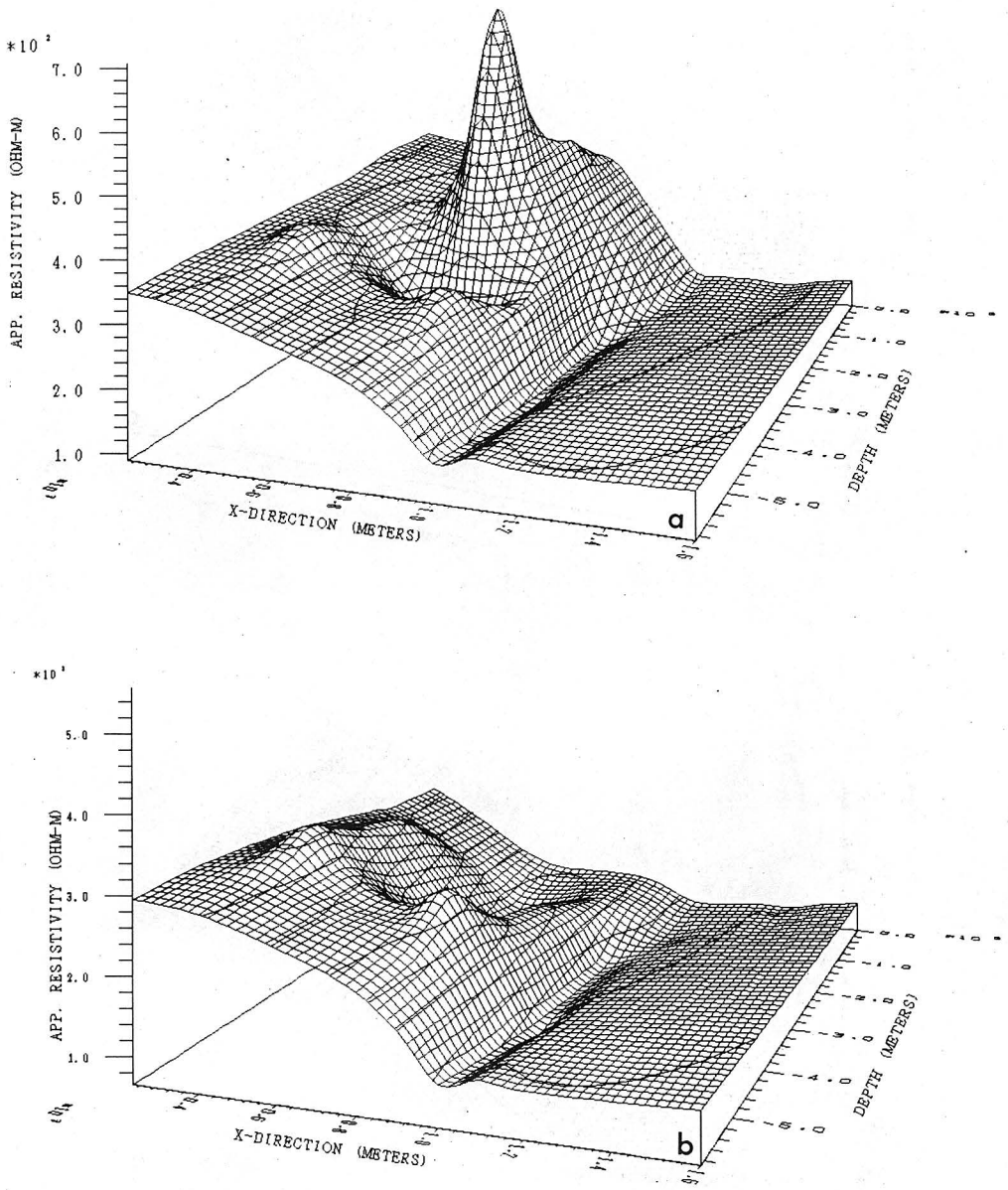

Fig. 9. Apparent resistivity three-dimensional perspective views of plot. (a): Perspective view of Figure 8a (Model 5272WLN), (b): Perspective view of Figure 8b(Model 5272WLC).

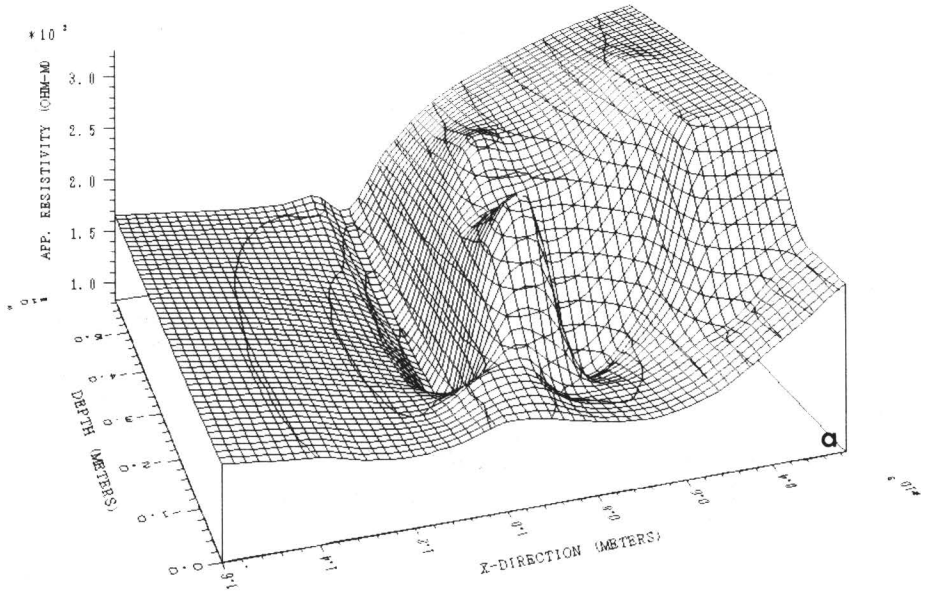
*10 ²
APP. RESISTIVITY (OHM-M)
3.0
2.5
2.0
1.5
1.0
DEPTH (METERS)
X-DIRECTION (METERS)
a

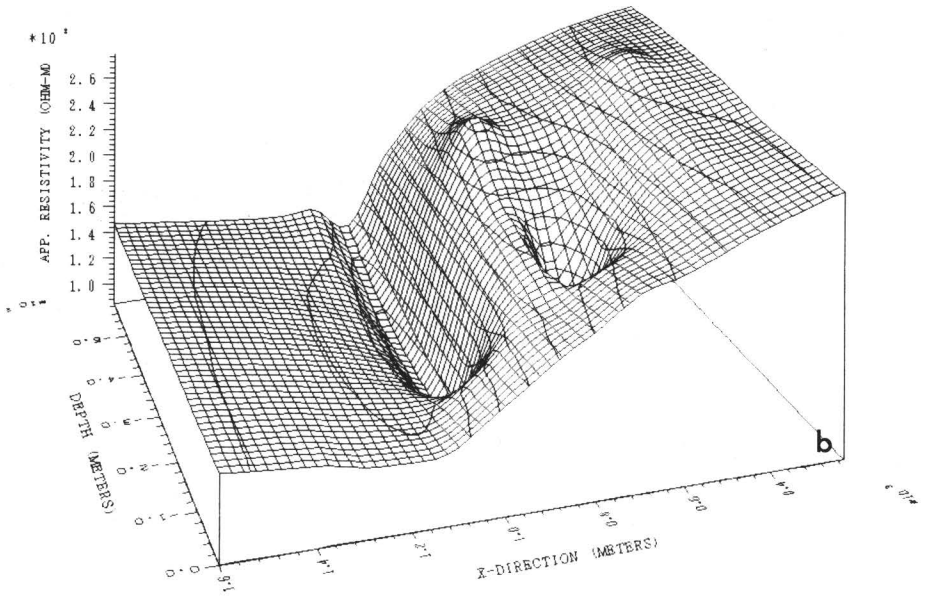
*10 ²
APP. RESISTIVITY (OHM-M)
2.6
2.4
2.2
2.0
1.8
1.6
1.4
1.2
1.0
DEPTH (METERS)
X-DIRECTION (METERS)
b

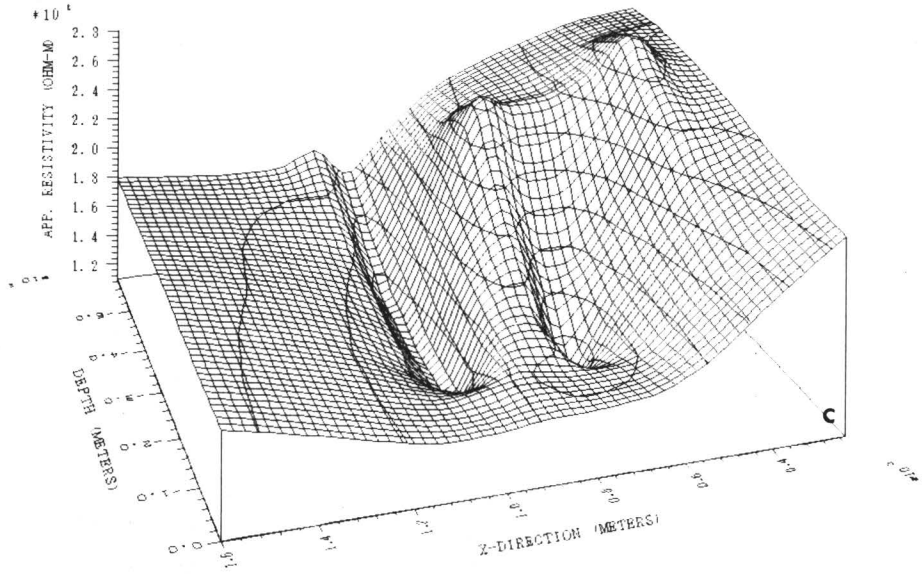

Fig. 10. Normalized apparent resistivity sections in the second stage of normalization procedure. (a) : Normalization result of Figure 9a by the apparent resistivity in the nontarget inhomogeneities model (Model WLN, $\rho_1=\rho_3=700$ ohm-m, $\rho_2=200$ ohm-m, $\rho_4=\rho_5=\rho_6=\rho_7=100$ ohm-m, $\rho_8=20$ ohm-m and $\rho_9=700$ ohm-m in Fig. 7), (b) : Normalization result of Figure 9b by the apparent resistivity in the nontarget inhomogeneities model (Model WLC, same as Model WLN except $\rho_9=20$ ohm-m in Fig. 7), (c) : Response due to Model 5272($\rho_1=700$ ohm-m, $\rho_2=200$ ohm-m, $\rho_3=10$ ohm-m and $\rho_4=\rho_5=\rho_6=\rho_7=\rho_8=\rho_9=100$ ohm-m in Fig. 7).

m, and Model WLC is almost the same as Model WLN except $\rho_9=20$ ohm-m. Figures 10 a and 10 b show the results of the normalization shown above. These normalized results are regarded as the second stage of the normalization procedure among three stages expected. Figure 10 c shows the apparent resistivity distribution for the model called Model 5272 which consists of a conductive target, a vertical contact and deep horizontal layers. This model is made by setting $\rho_1=700$ ohm-m, $\rho_2=200$ ohm-m, $\rho_3=10$ ohm-m, $\rho_4=\rho_5=\rho_6=\rho_7=\rho_8=\rho_9=100$ ohm-m in Figure 7. By comparing the normalized results shown in Figures 10 a and 10 b to the apparent resistivity distribution of the model with the target which is shown in Figure 10 c, it is recognized that the normalized section in Figure 10 a is more similar to the response due to Model 5272 in Figure 10 c than that of Figure 10 b. This difference is caused by the effect of a conductive material just above the target. Models WLN and WLC are made by assuming

that the resistivity distribution near the surface is clarified by the shallow electrical profilings or loggings. Therefore, in the second stage, the normalized results may be regarded as the response due to unknown deep resistivity structures.

Figures 11 a and 11 b illustrate the sensitivity difference contours at xz section obtained by Equation (8) for the normalized results shown in Figures 10 a and 10 b. In Figure 11 a, we can see the zone having a sensitivity difference of about 50% between the source and the top of the target, which position agrees with the maximum value in Figure 10 a. An increase of the normal sensitivity of about- 10% near the target is recognized. Also, the zone of sensitivity difference of about 30% above the source agrees with the high apparent resistivities produced at the respective positions in Figure 10 b.

Figures 12 a and 12 b are the results of the third stage process, that is, the

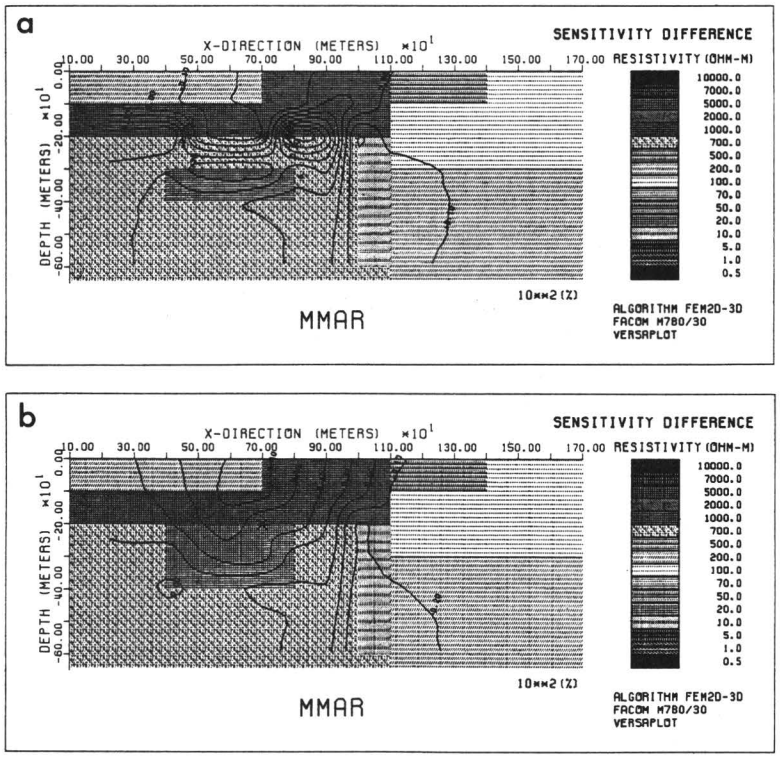

Fig. 11. Evaluation of interpretation process using the sensitivity difference in the second normalization stage. (a) : Evaluation of the normalization result shown in Figure 10a, (b) : Evaluation of the normalization result shown in Figure 10b.

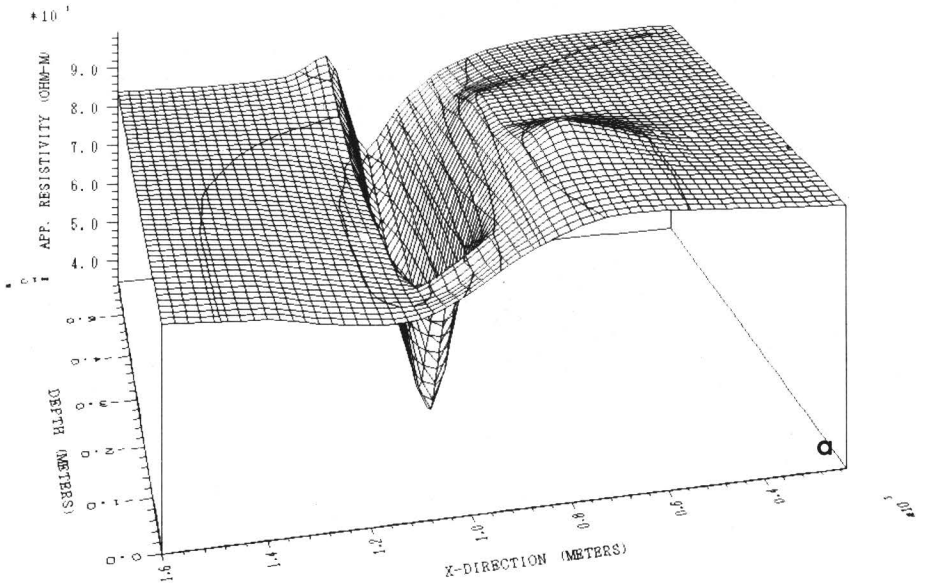
*10 1
APP. RESISTIVITY (OHM-M)
9.0
8.0
7.0
6.0
5.0
4.0
DEPTH (METERS)
0.0
0.1
0.2
0.3
0.4
0.6
1.6
1.4
1.2
1.0
0.8
0.6
0.4
*10 -1
X-DIRECTION (METERS)
a

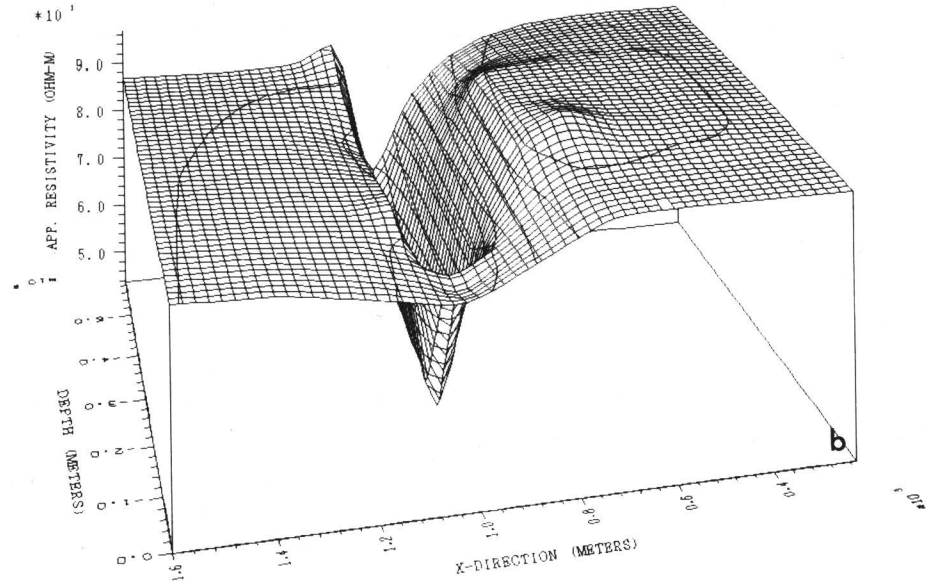
*10 1
APP. RESISTIVITY (OHM-M)
9.0
8.0
7.0
6.0
5.0
DEPTH (METERS)
0.0
0.1
0.2
0.3
0.4
0.6
1.6
1.4
1.2
1.0
0.8
0.6
0.4
*10 -1
X-DIRECTION (METERS)
b

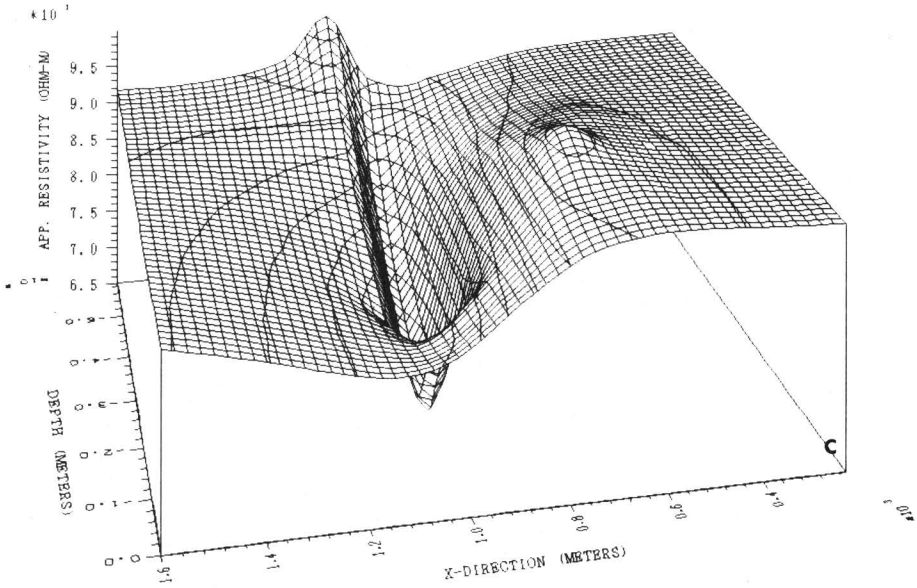

Fig. 12. Normalized apparent resistivity sections in the third stage of normalization procedure. (a) : Normalization result of Figure 9a by the apparent resistivity in the nontarget inhomogeneities model (Model 72WLN, $\rho_1=\rho_3=$ 700 ohm-m, $\rho_2=\rho_4=200$ ohm-m, $\rho_5=1000$ ohm-m, $\rho_6=100$ ohm-m, $\rho_7=500$ ohm-m, $\rho_8=20$ ohm-m and $\rho_9=700$ ohm-m in Fig. 7), (b) : Normalization result of Figure 9b by the apparent resistivity in the nontarget inhomogeneities model (Model 72WLC, same as Model 72WLN except $\rho_9=20$ ohm-m in Fig. 7), (c) : Response due to the target inhomogeneities model (Model 52, $\rho_1=\rho_2=100$ ohm-m, $\rho_3=10$ ohm-m and $\rho_4=\rho_5=\rho_6=\rho_7=\rho_8=\rho_9=100$ ohm-m in Fig. 7).

apparent resistivities shown in Figure 8 are normalized by the apparent resistivities of the model consisting of all the surrounding nontarget inhomogeneities. Those are Model 72 WLN and Model 72 WLC, respectively. The effects due to the nontarget inhomogeneities, such as vertical contact, near-surface and deep horizontal layers and near-suface local structure, have been almost clearly reduced in comparison with the second stage normalized results.

The response due to the target in the homogeneous half-space medium is presented in Figure 12 c. Both Figures 12 a and 12 b are similar to Figure 12 c, but Figure 12 b which is obtained in the case where the model has the near-source local noise structure ($\rho_9=$ 20 ohm-m) is more sensitive to the target than the result shown in Figure 12 a for the model which has no near-source local noise structure. The reverse characteristics of the sensitivity beneath the target in Figure 12 c have also been recognized in small rates in both Figures 12 a and 12

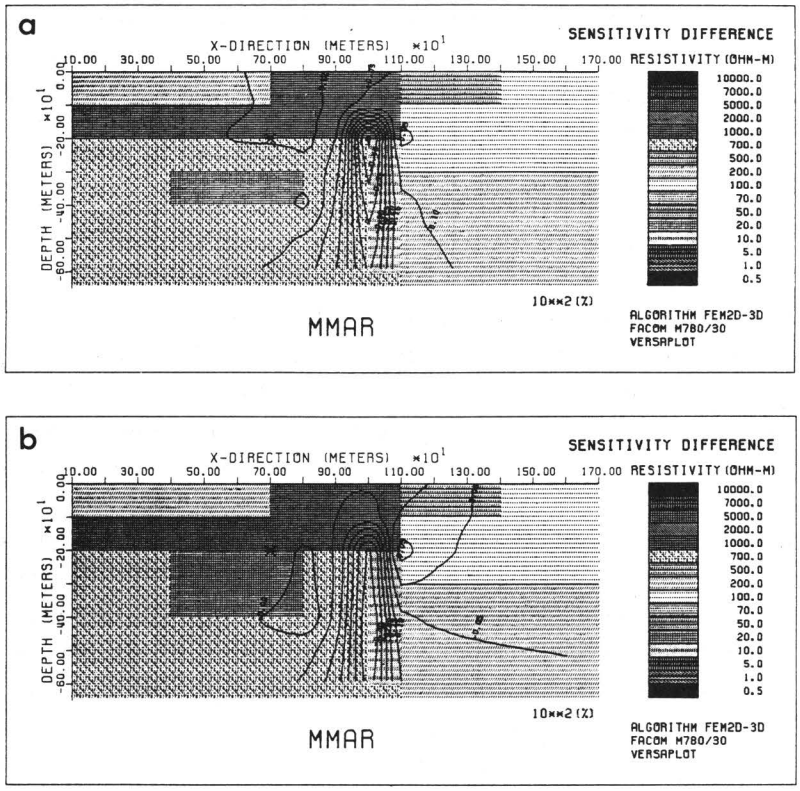

Fig. 13. Evaluation of interpretation process using the sensitivity difference in the third normalization stage. (a) : Evaluation of the normalization result shown in Figure 12a, (b) : Evaluation of the normalization result shown in Figure 12b.

b.

Finally, we have evaluated the normalized sections (Figs. 12 a and 12 b) using the sensitivity difference shown in Figures 13 a and 13 b. In was found that the third stage normalization procedure by all of the surrounding nontarget inhomogeneities reduced the effects of the noise structures. Also, it enhanced the response due to the target more clearly than the second stage normalization procedure which is performed by using the model consisting of a part of the resistivity environments. It is due to the fact that the mutual reactions among the nontarget structures in the third stage are larger than those in the second stage. The increases of about-20% in the normal sensitivity shown in Figures 13 a and 13 b indicate that the successful extraction and enhancement of the response due to the target is achieved.

Consequently, we have clarified that it is very useful to express the resistiv-

ity information in the interpretation process as the proper display, for an example, a three-dimensional perspective view of the plot as well as the two-dimensional contour, for monitoring and evaluating both the process and the results, and also as an aid to the interactive modeling system.

5. Construction of sensitivity distribution in nontarget inhomogeneities and its application

The future effectiveness of the resistivity method depends upon its ability to interpret data in more complex structure environments. Generally, the effects of nontarget surroundings such as weathered overburden layers, vertical contacts, faults, fracture zones, deep bed rocks or host rocks, near-surface lateral or local inhomogeneities and topography are noises, and the response due to the target is a signal.

In these various resistivity environments, one must be careful when applying homogeneous medium interpretation techniques. The sensitivity distributions in the case of homogeneous medium had been developed and reported in the papers[9-12], including Geophysical Exploration (Butsuri-Tanko in Japanese), Vol. 25 (1972). Barker (1978)[13], at Birmingham University, reported very interesting signal contribution sections similar to the sensitivity distributions in the Geophysical Journal of the Royal Astronomical Society, vol. 59. These concepts have been applied to practical problems in resistivity surveys and interpretation of the results.[1)12)]

However, recently we have recognized that it is very important to develop the sensitivity distribution in nontarget inhomogeneities for the improvement of resistivity interpretation techniques. Undoubtedly, if the sensitivity distribution in the homogeneous medium was equal to that of nontarget inhomogeneities, it can be applied to the resistivity interpretation of the various nontarget inhomogeneities.

But actually it is difficult to interpret the response due to the target with various surroundings using only the sensitivity distribution in the homogeneous medium. On the other hand, one must interpret not only the static resistivity information but also the dynamic resistivity information, such as various resistivity changes with time or with energy given naturally or artificially.

From the points of view shown above, it is very useful and interesting to acquire knowledge about the sensitivity characteristics in nontarget inhomogeneities. In this section 5, both the sensitivity distribution and the sensitivity difference in the nontarget inhomogeneities, including simple and

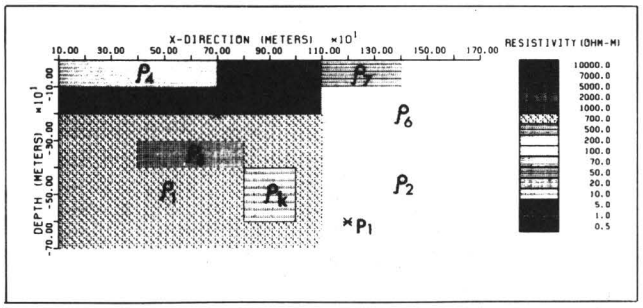

Fig. 14. An example illustrating the response due to unit volume target and electrode system in nontarget inhomogeneities.

complicated noise structures, have been defined and developed in order to find out a way to a more accurate interpretation of the resistivity methods and systems, and to offer exciting oppotunities for the detection of the target in practical problems.

Figures 15 a and 15 b show the examples of the sensitivity distributions as a three-dimensional perspective view of the plot when the target of resistivity ρ_k= 10 ohm-m exists in the simple nontarget inhomogeneities model (Model 71 W, ρ_1 $=\rho_5=\rho_8=$ 700 ohm-m, $\rho_2=\rho_6=\rho_7=$ 100 ohm-m and $\rho_4=$ 200 ohm-m in Fig. 14) and the more complicated nontarget inhomogeneities model (Model 72 WLN, $\rho_1=$ 700 ohm-m, $\rho_2=\rho_4=$ 200 ohm-m, $\rho_5=$ 1000 ohm-m, $\rho_6=$ 100 ohm-m, $\rho_7=$ 500 ohm-m and $\rho_8=$ 20 ohm-m in Fig. 14), respectively. Figure 15 c shows the perspective view of sensitivity distribution due to the target in the homogeneous medium. The electrode configuration is a kind of cross-hole array, namely, C (subsurface) P (subsurface) solid electrode arrangement used as an electrode array of so-called computerized geotomography (by analogy with medical tomography). These perspective views of sensitivity distributions can be obtained easily by using the PDB (Picture Data Base) system. We can display various plots such as automatic two-dimensional contour plots, bird's eye views and mixed expressions. The examples illustrated in Figures 15 a and 15 b have been obtained by using PDB S 71 WP 7. DATA and SWLNP 7. DATA. Comparing Figures 15 a and 15 b with Figure 15 c, we see that both of the sensitivity distributions in the simple nontarget inhomogeneities (Model 71 W) and in the more complicated one (Model 72 WLN) are quite similar to those in the case of the homogeneous medium except the detailed characteristics such as the tendency of reverse sensitivity zones between C_1 and P_1. It has been found that Figure 15 b is more similar to Figure 15 c than Figure 15 a at the zone of complicated structures.

The results of evaluation by the sensitivity difference method are presented

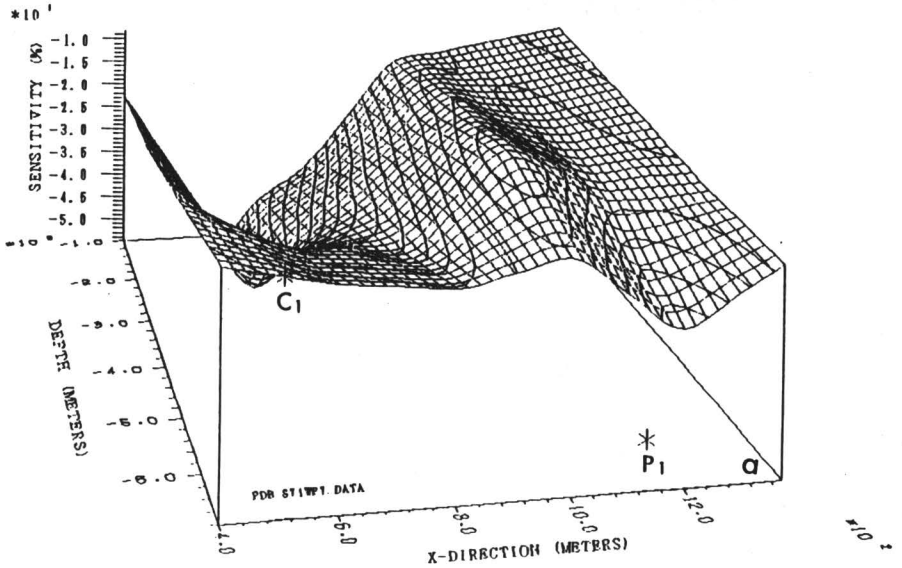
*10 '
SENSITIVITY (%)
-1.0
-1.5
-2.0
-2.5
-3.0
-3.5
-4.0
-4.5
-5.0
DEPTH (METERS)
C1
P1
a
PDB ST1WP1.DATA
X-DIRECTION (METERS)

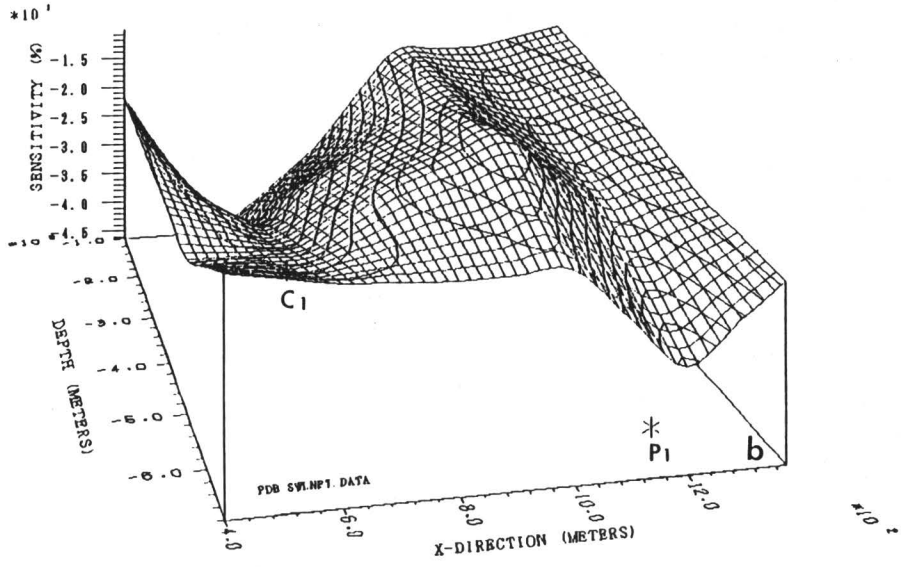
*10 '
SENSITIVITY (%)
-1.5
-2.0
-2.5
-3.0
-3.5
-4.0
-4.5
DEPTH (METERS)
C1
P1
b
PDB SV1.NP1.DATA
X-DIRECTION (METERS)

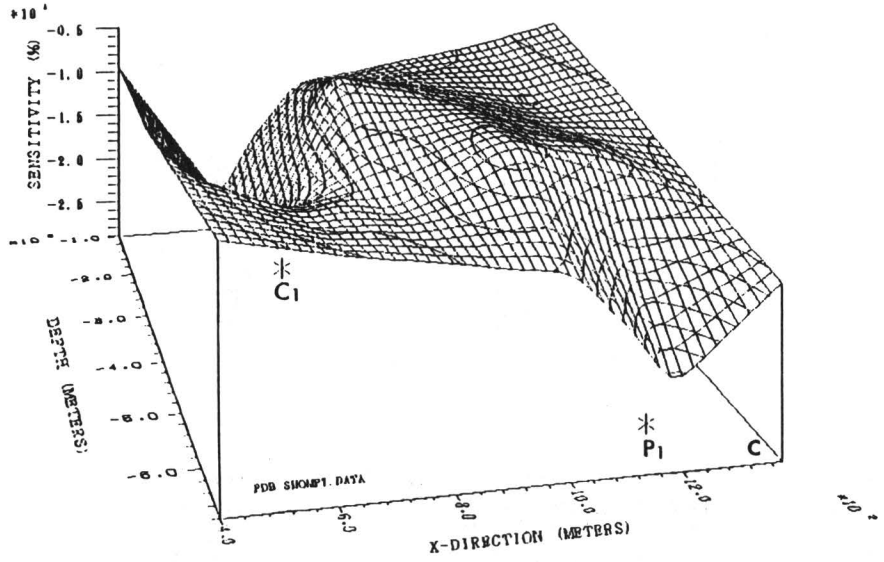

Fig. 15. Three-dimensional perspective views of the sensitivity distribution of C (subsurface) P(subsurface) solid electrode array. (a) : Sensitivity distribution due to target (ρ_k=10 ohm-m) in the nontarget inhomogeneities model (Model 71W, $\rho_1=\rho_3=\rho_5=\rho_8$=700 ohm-m, $\rho_2=\rho_6=\rho_7$=100 ohm-m and ρ_4=200 ohm-m in Fig. 14), (b) : Sensitivity distribution due to target(ρ_k=10 ohm-m) in the nontarget inhomogeneities model (Model 72WLN, ρ_1=700 ohm-m, $\rho_2=\rho_4$=200 ohm-m, ρ_5=1000 ohm-m, ρ_6=100 ohm-m, ρ_7=500 ohm-m and ρ_8= 20 ohm-m in Fig. 14). (c) : Sensitivity distribution due to target (ρ_k=10 ohm-m) in the homogeneous medium with resistivity of 100 ohm-m.

in Figures 16 a, 16 b, and 16 c. First, in comparing the simple inhomogeneities (Model 71 W) with the homogeneous case, the enhancements of the normal sensitivity of about- 28% near the source C_1 and above the potential electrode P_1 are clearly observed. Next, in comparing the complicated inhomogeneities (Model 72 WLN) with the homogeneous case, the enhancements of the normal sensitivity near the source C_1 and above the potential electrode P_1 are similar to those in Model 71 W. Also, the sensitivity differences are small near the local conductive noise structure with ρ_8= 20 ohm-m, and are large beneath the local noise structure near the source C_1. Figure 16 a in the case of Model 71 W shows the unbalanced normal sensitivity increase in the right and left sides of the vertical contact. Figure 16 b in the case of Model 72 WLN shows interesting characteristics of sensitivity averaging in the complicated structures.

It is interesting and reasonable that the sensitivity differences at the more

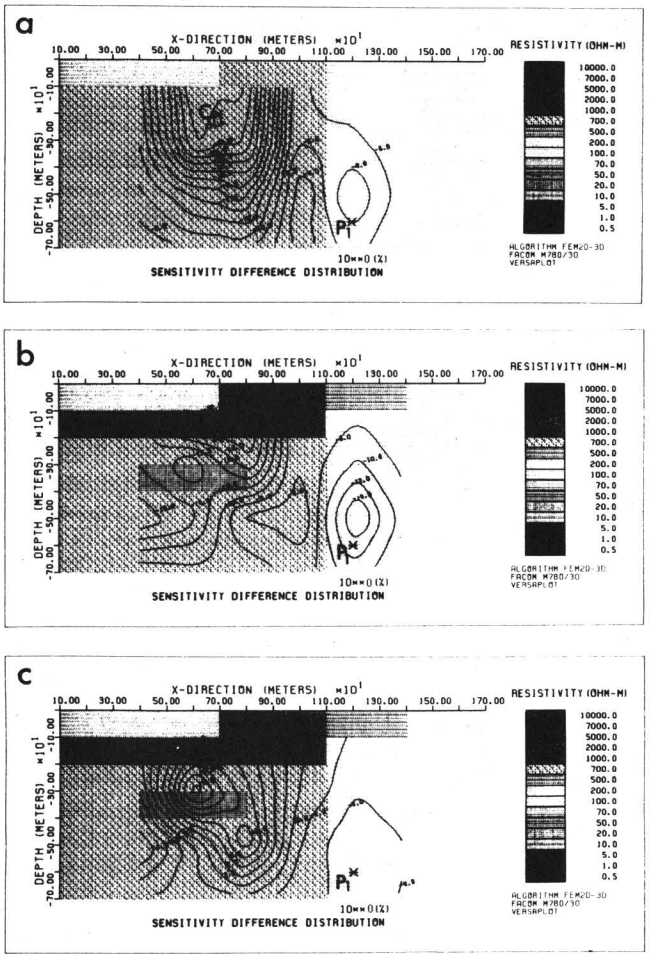

Fig. 16. Evaluation of nontarget inhomogeneity effects using the sensitivity difference. (a) : Difference distribution between Figures 15a and 15c, (b) : Difference distribution between Figures 15b and 15c, (c) : Difference distribution between Figures 15a and 15b.

complex nontarget inhomogeneities zone are smaller than those at the same zone of the simple nontarget inhomogeneities.

6. Conclusions

Recently, the growing use of computer simulation increases a demand for the investigations and the developments of interpretation methods.[36] Numerical modeling including the visualization technique and the use of subsurface electrodes have been new elements of most important recent developments in electrical survey methods. Also, electrical methods using subsurface electrodes have become increasingly more useful exploration tools for detecting deep or hidden mineral deposits, energy or groundwater resources and geological fracture zones, and also monitoring groundwater contamination, nuclear waste repository and various changes of earth structures.

In the future, the effectiveness of the electrical technique depends upon its ability to interpret the data obtained under more complex structure environments. Particularly, it is very important and interesting how to extract and enhance the response due to a target.

First, in order to reduce the effects of nontarget inhomogeneities we have studied a normalization procedure of the geologic structure noises using the FEM 2D-3D algorithm. As a result, we have found out that it is very useful to normalize the resistivity information by the background resistivity information.

Next, we have developed a new modeling algorithm including the visualization technique. Since it is important to monitor and evaluate the interpretation not only of results but also the process, we have studied an expression procedure, such as the traditional two-dimensional contour plot and the three-dimensional perspective view of plot using the interactive graphics system. The bird's eye view of resistivity information yields a more sensitive and higher density quantitative evaluation of the iterative interpretation process than only the numerical data.

Furthermore, the sensitivity distribution in nontarget inhomogeneities defined in this study contributes to a greater accuracy and resolution than only in the homogeneous medium. The sensitivity difference method may become an effective indicator to evaluate the simulation algorithms and the interpretation of the results and processes.

The examples of the interpretation procedure mentioned above appear to give an aid to extraction and enhancement of the response (signal) due to the target in various nontarget inhomogeneities for a new resistivity interpretation.

Acknowledgement

The numerical simulation and visualization were performed by the Fujitsu computer FACOM M 780 at the Data Processing Center of Kyoto University. This work was supported by the Grant-in-Aid for Scientific Research (6085116) of the Ministry of Education and Culture in Japan.

References

1) T. Sugano, Applications of electrical prospecting methods to mineral exploration and evaluation, presented at Ann. Mtg., MMIJ, A-3, pp. 7-11, 1982.
2) J. H. Coggon, Electromagnetic and electrical modeling by the finite element method, Geophysics, vol. 36, no. 1, pp. 132-155, 1971.
3) L. Rijo, Modeling of electric and electromagnetic data, Ph. D. dissertation, Univ. of Utah, pp. 1-242, 1977.
4) J. X. Zhao, L. Rijo and S. H. Ward, Effects of geologic noise on cross-borehole electrical surveys, Geophysics, vol. 51, no. 10, pp. 1978-1991, 1986.
5) T. Sugano, Electrical resistivity pilot survey using borehole solid electrode arrays, Seikan Tunnel Geophysical Exploration Commitee, Report 49-3 (in Japanese), pp. 22-23, 1974.
6) T. Sugano and K. Sassa, Cross-hole and hole-to-surface resistivity modeling, Geophysical Exprolation (Butsuri-Tansa in Japanese), vol. 41, no. 1, pp. 1-17, 1988.
7) T. Sugano and K. Sassa, Normalization procedure of nontarget inhomogeneities for resistivity interpretation, presented at Mtg. of Nondestructive Inspection (in Japanese), NDI-no. 3881, pp. 43-50, 1987.
8) D. F. Pridmore, Three dimensional modeling of electric and electromagnetic data using the finite element method, Ph. D. dissertation, Univ. of Utah, pp. 144-185, 1978.
9) T. Sugano, A fundamentary study on resistivity interpretation, Msc. thesis, Kyoto University, pp. 1-150, 1968.
10) E. Yoshizumi and T. Sugano, Sensitivity distribution of electrode configuration (I) Surface electrode arrays, Geophysical Exploration (Butsuri-Tanko in Japanese), vol. 25, no. 1, pp. 27-33, 1972.
11) T. Sugano and E. Yoshizumi, Sensitivity distribution in the case of valley topography, presented at Ann. Mtg., SEGJ, 4, pp. 5, 1976.
12) SEGJ, Sensitivity distribution, Encyclopedic dictionary of exploration geophysics (in Japanese), Society of Exploration Geophysicists of Japan, pp. 63-64, 1978.
13) R. D. Barker, Signal contribution sections and their use in resistivity studies, Geophysical Journal of the Royal Astronomical Soiety, no. 59, pp. 123-129, 1979.
14) F. W. Yang and S. H. Ward, On sensitivity of surface-to-borehole resistivity measurements to the attitude and the depth to center of a three-dimensional spheroid, Geophysics, vol. 50, no. 7, pp. 1173-1178, 1985.
15) J. J. Daniels, Hole-to-surface resistivity measurements, Geophysics, vol. 48, no. 1, pp. 87-97, 1983.

16) J. J. Daniels and A. V. Dyck, Borehole resistivity and electromagnetic methods applied to mineral exploration, IEEE Trans. on Geosci. and Remote Sensing, vol. GE-22, no. 1, pp. 80-87, 1984.

17) W. Daily, Underground oil-shale retort monitoring using geotomography, Geophysics, vol. 49, no. 10, pp. 1701-1707, 1984.

18) J. E. Acosta and M. H. Worthington, A borehole magnetometric resistivity experiment, Geophysical Prospecting, vol. 31, no. 5, pp. 800-809, 1983.

19) R. C. Fox, G. W. Hohmann, T. J. Killpack and L. Rijo, Topographic effects in resistivity and induced-polarization surveys, Geophysics, vol. 45, no. 1, pp. 75-93, 1980.

20) H. T. Holcombe and G. R. Jiracek, Three-dimensional terrain corrections in resistivity surveys, Geophysics, vol. 49, no. 4, pp. 439-452, 1984.

21) SEG, Pseudosection, Encyclopedic dictionary of exploration geophysics, Society of Exploration Geophysicists, 2nd ed., pp. 192-193, 1984.

22) D. R. Word, R. Gross and D. M. Chambers, An EMAP case study, presented at the 56th Ann. Internat. Mtg., SEG, Houston, pp. 61-63, 1986.

23) R. C. Robertson, The electromagnetic response of a heterogeneous layer modeled by two thin sheets in a uniformly conduction half-space, IEEE Trans. on Geosci. and Remote Sensing, vol. GE-26, no. 1, 1988.

24) J. F. Hermance, Efficient modeling of 3-D magnetotelluric field in complicated basin structures, presented at the 56th Ann. Internat. Mtg., SEG, Houston, pp. 74-79, 1986.

25) L. Alfano, Geoelectric prospecting with underground electrodes, Geophysical Prospecting, vol. 10, no. 3, pp. 290-303, 1962.

26) R. H. Merkel and S. S. Alexander, Resistivity analysis for models of a sphere in a half-space with buried current souces, Geophysical Prospecting, vol. 19, no. 4, pp. 640-651, 1971.

27) A. Jämtlid, K. A. Magnussen, O. Olsson and L. Stenberg, Electrical borehole measurements for the mapping of fracture zones in crystalline rocks, Geoexploration, vol. 22, no. 3. 4, pp. 203-216, 1984.

28) D. Arandjelovic, Resistivity method applied to the investigation of earth embankments, First Break, EAEG, vol. 4, no. 3, pp. 19-23, 1986.

29) M. R. Lewis and F. P. Haeni, The use of subsurface geophysical techniques to detect fractures in bedrock, U. S. Geological Survey Circular, 987, pp. 1-14, 1987.

30) D. L. Masne and C. Poirmeur, Three-dimensional model results for an electrical hole-to-surface method: Application to the interpretation of a field survey, Geophysics, vol. 53, no. 1, pp. 85-103, 1988.

31) K. Vozoff, Numerical resistivity interpretation: General inhomogeneity, Geophysics, vol. 25, no. 6, pp. 1184-1194, 1960.

32) N. C. Smith and K. Vozoff, Two-dimensional DC resistivity inversion for dipole-dipole data, IEEE Trans. on Geosci. and Remote Sensing, vol. GE-22, no. 1, pp. 21-28, 1984.

33) R. J. Lytle, Resistivity and induced polarization probing in the vicinity of a spherical anomaly, IEEE Trans. on Geosci. and Remote Sensing, vol. GE-20, no. 4, pp. 493-499, 1982.

34) M. L. Oristaglio and M. H. Worthington, Inversion of subsurface and borehole electromagnetic data for two-dimensional electrical conductivity models, Geophysical Pro-

specting, vol. 28, no. 4, pp. 633 - 657, 1980.

35) M. H. Worthington, An introduction to geophysical tomography, First Break, EAEG, vol. 2, no. 11, pp. 20 - 26, 1984.

36) T. Sugano and K. Sassa, Expression procedure in an evaluation of resistivity interpretation process, Geophysical Exploration (Butsuri-tansa in Japanese), vol. 41, no. 2, pp. 116 - 132, 1988.

37) M. P. Curtis, A. C. Gerhardstein and R. E. Howard, Interpretation of large 3-D data volumes, presented at the 56 th Ann. Internat. Mtg., Society of Exploration Geophysicists, Houston, pp. 497 - 499, 1987.